

## Impact of sea grass density on carbonate dissolution in Bahamian sediments

David J. Burdige

Department of Ocean, Earth, and Atmospheric Sciences, Old Dominion University, Norfolk, Virginia 23529

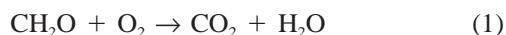
Richard C. Zimmerman

Moss Landing Marine Laboratories, California State University, Moss Landing, California 95039

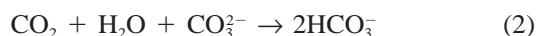
### Abstract

Carbonate dissolution has been widely observed in shallow water tropical sediments. However, sediment budgets have generally not been closed with respect to the amount of acid required to produce the observed carbonate dissolution. Recently it has been suggested that enhanced oxygen transport into sediments through the roots and rhizomes of sea grasses might play a role in resolving this mass balance problem. We conducted studies of sea grass–carbonate sediment interactions around Lee Stocking Island, Exuma Islands, Bahamas to further examine this problem. Our studies showed that alkalinity, total dissolved inorganic carbon ( $\Sigma\text{CO}_2$ ) and  $\text{Ca}^{2+}$  increased with depth in the pore waters, while pH and calculated carbonate ion concentration decreased with depth. These observations are consistent with the occurrence of carbonate dissolution in these sediments. The magnitude of pore water alkalinity,  $\Sigma\text{CO}_2$ , and  $\text{Ca}^{2+}$  changes was also related to sea grass density, with the largest gradients seen in the sediments of dense sea grass beds. Calculations suggested that less than ~50% of the  $\text{O}_2$  needed to drive aerobic respiration (and ultimately carbonate dissolution via  $\text{CO}_2$  production) could be supplied by transport processes such as diffusion, bioturbation, and physical pore water advection. Furthermore, the  $\text{O}_2$  needed to balance the carbonate dissolution budget could be provided by the transport of <15% of the photosynthetically derived  $\text{O}_2$  to the sediments through sea grass roots and rhizomes without enhancing the removal of carbonate dissolution end products. Thus sea grasses play an important role in controlling the rates of carbonate dissolution in shallow water tropical marine sediments.

The dissolution of calcium carbonate in marine sediments is an important component of the oceanic and global carbon cycle on a variety of spatial and temporal scales (e.g., Morse and Mackenzie 1990; Milliman 1993). Carbonate dissolution occurs in aerobic sediments as a result of aqueous  $\text{CO}_2$  production during oxic remineralization of sediment organic matter (SOM, or  $\text{CH}_2\text{O}$  here), expressed here approximately as



(ignoring any alkalinity contributions associated with N and P remineralization, as well as acid production associated with the oxidation of metal sulfides such as  $\text{FeS}$ ). In sediments overlain by bottom waters supersaturated with respect to calcium carbonate, the metabolic acid produced by this reaction is first neutralized by titration with dissolved carbonate ion (e.g., Emerson and Bender 1981), producing bicarbonate according to,

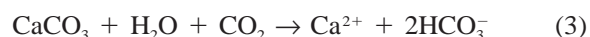


<sup>1</sup> Corresponding author (dburdige@odu.edu).

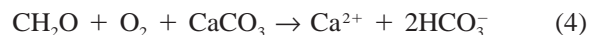
### Acknowledgments

Many thanks to K. Gardner, S. Kline, D. Kohrs, S. Palacios, J. P. Simjouw, and S. Wittlinger for their assistance in the field and in the lab. Thanks also go to the other CoBOP participants (especially chief scientist Charlie Mazel) for their camaraderie during five field expeditions to Lee Stocking Island, and to the Caribbean Marine Research Center for extensive logistical support. J. Middelburg, L. Walter and an anonymous reviewer provided important comments and suggestions that greatly improved the quality of this manuscript. Financial support was provided by the Environmental Optics Program, Office of Naval Research (CoBOP DRI).

This consumption of  $\text{CO}_3^{2-}$  by Eq. 2 lowers the saturation state of the pore waters. Once the pore waters become sufficiently undersaturated, dissolution of the most soluble carbonate mineral occurs according to the reaction,



The net reaction (i.e., the sum of Eqs. 1 and 3) can therefore be expressed as



which increases both the alkalinity and total dissolved inorganic carbon ( $\Sigma\text{CO}_2$ ) concentration of the pore waters.

Sulfate reduction is generally the next most significant SOM remineralization process in shallow water, tropical carbonate sediment after aerobic respiration (e.g., see discussions in Walter and Burton 1990). However, in contrast to aerobic respiration, sulfate reduction produces alkalinity and eventually leads to carbonate mineral supersaturation (Morse and Mackenzie 1990).

Carbonate dissolution has been documented in shallow water sediments using chemical, isotopic, and mineralogical techniques (Berner 1966; Morse et al. 1985, 1987; Moulin et al. 1985; Walter and Burton 1990; Rude and Aller 1991; Walter et al. 1993; Ku et al. 1999). In the work of Walter and coworkers in Florida Bay carbonate sediments (Walter and Burton 1990; Walter et al. 1993; Ku et al. 1999) it has also been observed that acid generation via aerobic respiration (Eq. 1) or oxidation of reduced iron and sulfur species (i.e., direct  $\text{H}^+$  production) was insufficient to explain the observed carbonate dissolution inferred from  $\text{Ca}^{2+}/\text{Cl}^-$  pore water profiles. Since both of these acid-generation processes require  $\text{O}_2$ , these results imply a significant discrepancy between rates of  $\text{O}_2$  transport into Florida Bay sediments and

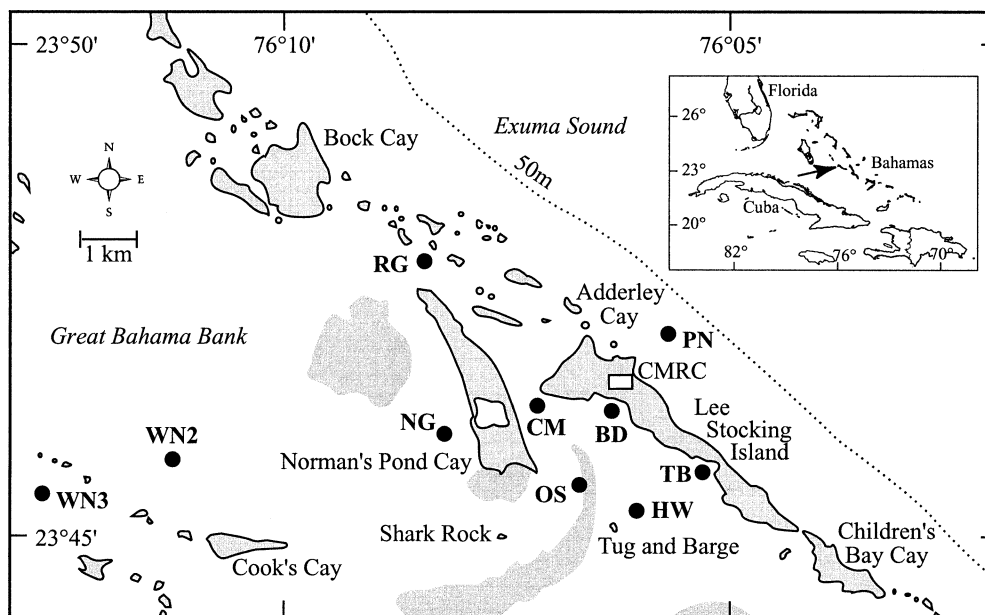


Fig. 1. A map of the LSI area and sampling sites. Site names and abbreviations: Twin Beaches (TB), Half Way (HW), Boat Dock (BD), Channel Marker (CM), Ooid Shoals (OS), Norman's Grapestones (NG), West of Norman's (WN), Rainbow Gardens (RG), and North Perry Reef (PN).

observed rates of sediment carbonate dissolution. Although bioturbation (e.g., Aller 1982) or pressure-induced pore water advection through such permeable sediments (e.g., Huettel and Webster 2001) may enhance transport of dissolved oxygen into sediments, these processes will also transport carbonate dissolution end products (e.g.,  $\text{Ca}^{2+}$  or excess alkalinity) out of sediments. Therefore, they likely cannot generate the previously observed stoichiometric discrepancies between sediment  $\text{O}_2$  input and carbonate dissolution.

Recently, Ku et al. (1999) suggested that  $\text{O}_2$  transport into sediments by sea grasses (submerged vascular plants) may provide the necessary oxygen input to balance these carbonate dissolution budgets (also see Eldridge and Morse 2000). In temperate clastic sediments *Zostera marina* (eel grass) is known to transport  $\text{O}_2$  through its roots and rhizomes to the surrounding sediments, markedly affecting redox conditions in the rhizosphere (Sand-Jensen et al. 1982; Smith et al. 1984; Jaynes and Carpenter 1986; Pedersen et al. 1998). Sea grasses such as *Thalassia testudinum* are characterized by a significant amount of below-ground biomass and may transport photosynthetically derived  $\text{O}_2$  into tropical carbonate sediments, thereby providing the missing  $\text{O}_2$  needed to balance the carbonate dissolution budget without enhancing the removal of carbonate dissolution end products.

In light of these observations, we examined carbonate dissolution in shallow tropical sediments of the Bahamas to determine whether there was a relationship between sea grass density, organic matter remineralization, and carbonate dissolution. This effort represents the first step in quantitatively establishing the importance of these submerged aquatic angiosperms in the diagenetic processes affecting tropical carbonate sediments. Such interactions are not only important from the standpoint of the biogeochemistry of the car-

bonate sediment-sea grass system, but can also have significant impacts on regional and global carbon cycles.

## Methods and materials

**Field sites**—Field studies were conducted in shallow water carbonate sediments around Lee Stocking Island (LSI), Exuma Islands, Bahamas (Fig. 1) using the Caribbean Marine Research Center (CMRC) as our base of operation. Five sampling expeditions (1–3 weeks in duration) were undertaken during 1998–2000 and will be referred to here as LSI 1 (May–June 1998), LSI 2 (January 1999), LSI 3 (May 1999), LSI 4 (January 2000), LSI 5 (May 2000).

Sites around LSI comprise a broad range of shallow tropical environments (also see discussions in Dill 1991). These include unvegetated well-sorted oolitic sands (i.e., ooids being spherical or elliptical carbonate grains that often have an internal radial or concentric [laminated] structure), sea grass meadows (mostly *Thalassia testudinum* or turtle grass) of densities exceeding 500 shoots  $\text{m}^{-2}$  (Table 1), grapestone deposits (i.e., clusters of oolitic particles and carbonate skeletal remains cemented together by microbial biofilms), and bioturbated sediments containing extensive *Callianassa* sp. (shrimp) mounds. Water depths at these sites range from 2 to 20 m.

Dense sea grass meadows were vegetated by relatively tall shoots (>25 cm) comprised of 3 to 5 leaves each. Sparse areas supported only slightly fewer shoots, but the shoots were much shorter (<20 cm) and were comprised of 2–3 leaves per shoot. Thus the large differences in leaf area index (LAI) and standing biomass reported in Table 1 resulted more from differences in shoot size than in shoot density. Vertical short shoots of these plants penetrated to ~20-cm

Table 1. Turtle grass densities and metabolic rates around Lee Stocking Island.

Sites	Shoot density (shoots cm <sup>-2</sup> )*	Leaf area index (LAI) (m <sup>2</sup> leaf m <sup>-2</sup> )	Leaf biomass (gdw m <sup>-2</sup> )
Dense turtle grass sites (most CM sites)†	497 ± 198 (226–958)	1.7 ± 0.6 (1.0–4.0)	349 ± 123 (206–791)
Sparse turtle grass sites (some CM sites, as well as HW and RG sites)†	339 ± 141 (70–690)	0.6 ± 0.2 (0.1–1.0)	112 ± 41 (19–195)
	January 1999	May 1999	
Light-saturated photosyntheses of turtle grass leaves (net) (μmol O <sub>2</sub> gdw <sup>-1</sup> h <sup>-1</sup> )	57 ± 21	108 ± 27	
Sea grass O <sub>2</sub> production (mmol O <sub>2</sub> m <sup>-2</sup> d <sup>-1</sup> ‡)			
Dense sea grass sites	198	377	
Sparse sea grass sites	64	122	

\* Values in parentheses are observed in range in these quantities. Unless indicated, all areas (m<sup>2</sup>) are for seafloor bottom.

† See Fig. 1 for site abbreviations.

‡ Obtained by multiplying the area-specific leaf biomass and light-saturated photosynthesis rates, assuming that these plants photosynthesize at light-saturated rates for 10 h d<sup>-1</sup>.

depth where they were attached to horizontal rhizomes. Roots extended beyond this 20-cm sediment depth.

The sediments around LSI are fine- to coarse-grained carbonate sands (~200–800-μm grain size) dominated by aragonite (~80%) and high-Mg calcite (~20%). Visual observations (Reid and Louchar, Univ. Miami, RSMAS, unpubl. data) indicated that the sediments are comprised of biogenic skeletal debris (mollusks, coral, red and green algae, calcareous sponges, and foraminifera), ooids, peloids (carbonate pellets of undetermined origin), and grapestones. Total organic carbon in these sediments is quite low (generally less than 0.5%; F. Dobbs, Old Dominion Univ., unpubl. data), typical of other Bahama Bank sediments (Morse et al. 1985). Sediment porosities ( $\phi$ ) range from ~50 to 80%.

*Sample collection and fractionation*—Diver-operated in situ pore water samplers, or sippers (Fig. 2), were designed to overcome difficulties in obtaining pore waters from sandy sediments (Marinelli et al. 1998; Berg and McGlathery 2001). These sippers are similar in design to pore water samplers described recently by Berg and McGlathery (2001).

Each sipper was fitted with a piece of 3.18-mm (outer diameter) Teflon tube of different lengths (*see below*) that contained a small piece of porous polypropylene rod inserted into the lower end of the tube. Each rack contained four sippers mounted on a small plate (15 × 30 cm), and the upper ends of the sipper tubes were attached to bulkhead fittings that screwed into (and through) the plate. The other end of each bulkhead fitting was attached to a three-way stopcock and a 10-ml glass, gas-tight syringe with a Luer-Lok connector. Syringes were held rigidly in the rack and attached to metal springs that drew a pore water sample into the syringe by pulling the plunger. During LSI 3, 4, and 5

we deployed pairs of sipper racks side-by-side, one rack fitted with tubes of 1, 2, 5, and 10 cm in length and the other fitted with tubes of 4, 8, 15, and 20 cm in length. During LSI 1 and 2 only sippers with 1-, 2-, 5-, and 10-cm sampling tubes were used.

To use the sippers a diver gently inserted the sample tubes into the sediments, and the dead volume in each tube was cleared with an auxiliary syringe. The three-way stopcock was rotated and a safety lever released, drawing samples from each sediment depth into the spring-loaded syringes. Filled syringes were sealed in situ by rotating the three-way stopcock again, and the samplers were returned to the surface. Sample syringes were stored on ice in the dark and returned to the lab within an hour of collection. A sample of overlying bottom water was also collected by the diver, along with each pore water profile, by filling and sealing a 50-ml syringe in situ.

At the CMRC lab, samples for analyses other than O<sub>2</sub> were filtered through 0.45-μm membrane filters and aliquoted into storage vessels. Samples for O<sub>2</sub> analyses were immediately analyzed as described in the next section. Control experiments indicated that these sealed glass syringes gained only 6–10 μM O<sub>2</sub> during the time (1 to 2 h) between collection and analysis. Total alkalinity and pH samples were filtered directly into 3-ml plastic syringes without exposure to air, sealed, and stored in a refrigerator until analyzed (within 2 d of collection). Samples for ΣCO<sub>2</sub> analyses were filtered into 1.5-ml glass serum vials and crimp-sealed shut with no headspace. These samples were stored refrigerated until analyzed at Old Dominion University within 2 months. Past work has shown that samples stored in this fashion are stable for this time period (Burdige and Homstead 1994). Samples for sulfate analyses were filtered into 1.5-ml snap-

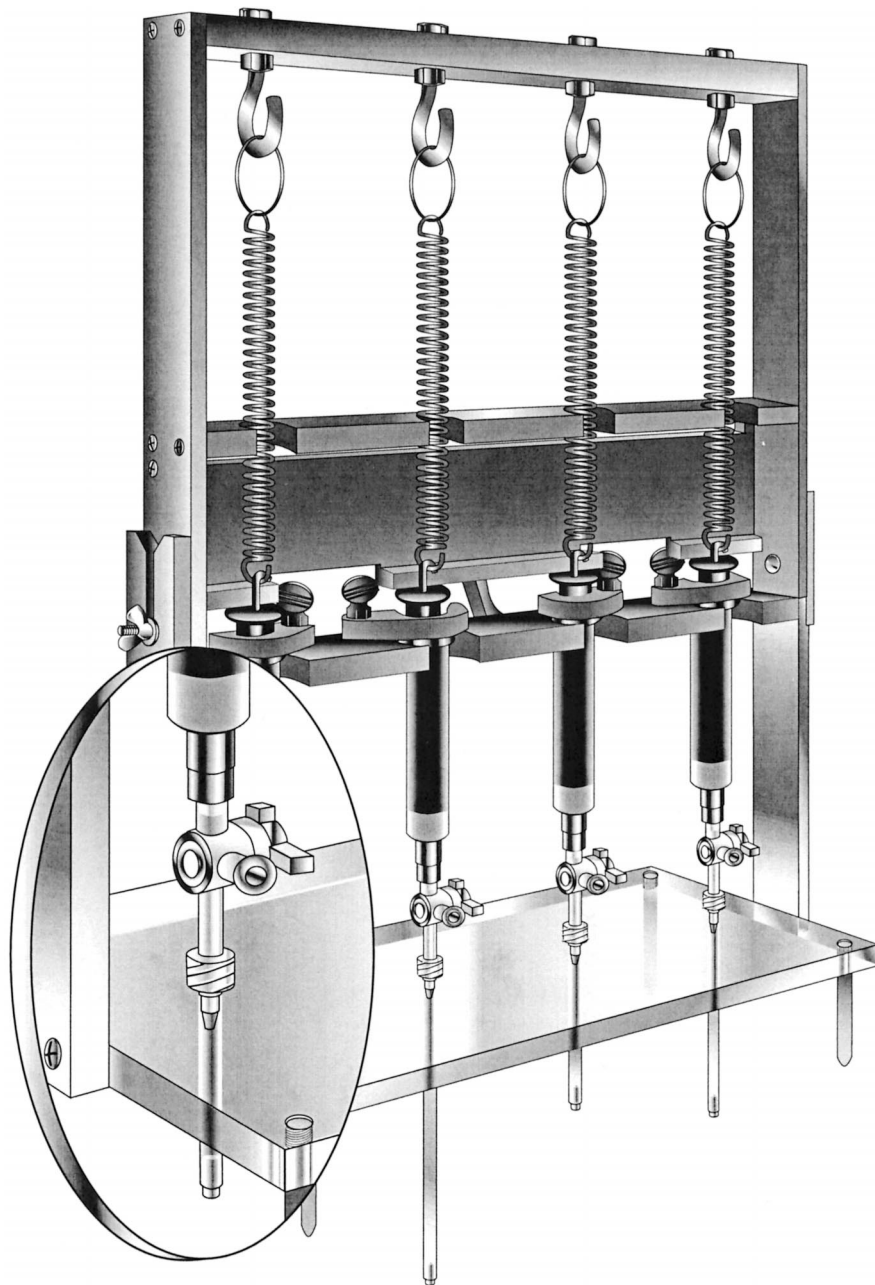


Fig. 2. A schematic diagram of the sediment sippers used to collect pore water samples in LSI sediments.

cap centrifuge tubes, acidified with  $25 \mu\text{l}$  of 6 N HCl, and stored refrigerated until analyzed.

Using an equation presented in Berg and McGlathery (2001), we estimate that the collection radius for our samplers is on the order of 1.5 cm. Laboratory tracer experiments with these samplers also showed that the uppermost (1-cm depth level) sipper entrains  $\sim 40\text{--}50\%$  overlying water ( $54 \pm 20\%$ ), with only  $\sim 20\%$  ( $24 \pm 11\%$ ) bottom water found in samples collected between 2 and 8 cm (the maximum depth used in these tracer experiments; Kline and Burdige pers. comm.). Overall, these observations indicate that the samplers are adequate to resolve biogeochemical pro-

cesses occurring in the upper  $\sim 20$  cm of LSI sediments (also see *Uncertainty of Pore Water Measurements* for further details).

*Pore water analyses*—Total alkalinity was determined by Gran titration (Gieskes et al. 1991). Pore water pH values were determined using a combination pH electrode calibrated with NIST-traceable buffers. For samples collected on trips LSI 1–4,  $\Sigma\text{CO}_2$  was determined using a flow injection technique (Lustwerk and Burdige 1995), while samples collected during LSI 5 were determined by coulometry using a UIC model CM5014  $\text{CO}_2$  coulometer (DOE 1994). For sam-

ples collected during LSI 5 dissolved calcium was determined by flame atomic absorption spectrophotometry after 100- to 150-fold dilution with 0.1% KCl. Sulfate was determined by ion chromatography. Salinity was determined by refractometry.

Dissolved oxygen was determined (during LSI 5) using a stirred polarographic electrode mounted in the base of a small volume (~5 ml) temperature-controlled chamber sealed with a gasketed top. Pore water was introduced into the bottom of the chamber using a small piece of tubing directly attached to the tip of the glass syringe from a sipper. The chamber was overfilled and sealed immediately prior to the O<sub>2</sub> measurement.

*Uncertainty of pore water measurements*—In the majority of the pore water profiles discussed here, we examined these profiles as a function sea grass density. This was done by collecting cores at different sites around LSI and then using them to determine average pore water profiles in dense sea grass sediments, sparse sea grass sediments, and bare oolitic sands (i.e., no sea grass; see Table 1 for further details). With this approach we observed that the relative and absolute standard deviations of average pore water values were much greater than the analytical uncertainties associated with individual measurements. This is largely due to the spatial heterogeneity that is typical of such sea grass environments, although variable bottom water entrainment in these pore water samples during collection also contributes to this uncertainty (see the discussion above). Average values of these standard deviations were: alkalinity,  $\pm 0.47$  mEq L<sup>-1</sup> or  $\pm 15\%$  (RSD);  $\Sigma\text{CO}_2$ ,  $\pm 0.44$  mM or  $\pm 14\%$ ; pH,  $\pm 0.24$  pH units or  $\pm 15\%$ ; salinity,  $\pm 0.75$  or  $\pm 2\%$ ; sulfate,  $\pm 1.3$  mM or  $\pm 4\%$ ; oxygen,  $\pm 34$   $\mu\text{M}$  or  $\pm 50\%$ ; calcium,  $\pm 0.43$  mM or  $\pm 4\%$ . In the remainder of this paper we will use these environmental uncertainties in our discussion and analysis of the data.

*Sea grass density and productivity measurements*—Shoot density was determined by divers at each site by direct counts of all shoots within 20 randomly located 0.1 m<sup>2</sup> quadrats. One shoot was collected from each quadrat for determination of leaf morphometrics and shoot biomass. Lengths of all leaves on each shoot were measured to the nearest mm with a plastic meter tape. Leaf widths were measured to the nearest 0.01 mm using a digital caliper. Shoot-specific leaf area was calculated as the sum of the one-sided area (length  $\times$  width) of all leaves on each shoot. Leaf area index (LAI) was then calculated as the product of shoot density (shoots m<sup>-2</sup>) and shoot-specific leaf area (m<sup>2</sup> leaf area shoot<sup>-1</sup>). Shoots were dried for 36 h at 60°C and weighed for determination of dry mass–leaf area relationships.

Rates of oxygenic leaf metabolism were measured using temperature-controlled polarographic chambers. Photosynthesis versus irradiance curves were determined using at least 10 irradiances provided by a quartz-halogen lamp and neutral density filters. Respiration was determined by measuring O<sub>2</sub> consumption in the dark. All measurements were performed at ambient temperatures (25–30°C) determined at the time of shoot collection. Data were fit to the exponential function of Webb et al. (1974) using nonlinear regressions

and parameter error estimates described by Zimmerman et al. (1987).

*Carbonate speciation calculations*—Pore water and bottom water carbonate ion concentrations were calculated with total alkalinity,  $\Sigma\text{CO}_2$ , and pH data using the program CO2SYS (v. 1.05; Lewis and Wallace 1998) and the carbonic acid dissociation constants of Roy et al. (1996). Since this program requires only two CO<sub>2</sub> system parameters to determine carbonate speciation, we carried out calculations using all three pairs of parameters (i.e., alkalinity and  $\Sigma\text{CO}_2$ , alkalinity and pH, and  $\Sigma\text{CO}_2$  and pH) and then averaged the results to obtain pore water carbonate ion concentrations in individual samples. For our entire data set ( $n = 320$  samples) the three calculated carbonate ion concentrations for a given sample agreed to within  $\pm 33$   $\mu\text{M}$  or  $\pm 20\%$ .

*Diffusive flux and rate calculations*—Diffusive fluxes across the sediment–water interface were determined using pore water data and Fick's First Law ( $J = -\phi D_s dC/dx_{x=0}$ ). The interfacial gradient ( $dC/dx_{x=0}$ ) was estimated by linear regression of pore water data in the upper 5 cm of sediment. Bulk sediment diffusion coefficients ( $D_s$ ) were estimated using the equation  $D_s = \phi D^\circ$  (Ullman and Aller 1982), with  $D^\circ$  values taken from Boudreau (1997). The bicarbonate diffusion coefficient was used in both alkalinity and  $\Sigma\text{CO}_2$  flux calculations. Depth-integrated rates of sediment carbon oxidation ( $C_{\text{ox}}$ ) were determined with alkalinity and  $\Sigma\text{CO}_2$  diffusive fluxes using the equation  $C_{\text{ox}} = \Sigma\text{CO}_2 \text{ Flux} - 0.5 \cdot \text{Alk Flux}$  (based on Eq. 4; also see Berelson et al. 1996, for further details). Assuming no net sulfate reduction, the depth-integrated rate of carbonate dissolution (again based on Eq. 4) is  $0.5 \cdot \text{Alk Flux}$ .

## Results and discussion

*General trends in the pore water data*—Alkalinity and  $\Sigma\text{CO}_2$  pore water profiles in LSI sediments generally increased with depth, while pH and calculated carbonate ion concentrations decreased with sediment depth (Figs. 3 and 4). These profiles, along with pore water DOC and DOM fluorescence profiles from these sites (Kline and Burdige pers. comm.), all generally had relatively flat gradients in the upper ~2–4 cm, as compared to gradients in the deeper sediments. This likely occurs as a result of pressure-induced pore water advection in these coarse-grained sediments and suggests that any rates of sediment processes determined with these pore water profiles will be minimum estimates of their true values.

To further examine whether pore water advection is a likely explanation for these observations, the permeability of LSI sediments was calculated with the Carmen-Kozeny equation, assuming spherical particles (Huettel and Webster 2001). With observed sediment grain sizes and porosities, calculated permeabilities in LSI sediments were greater than ~200 Darcys. In sediments where permeabilities exceed ~1–20 Darcys, pore water advection through the sediments, due to near seabed pressure gradients caused by surface roughness or biogenic structures, is thought to be a signifi-

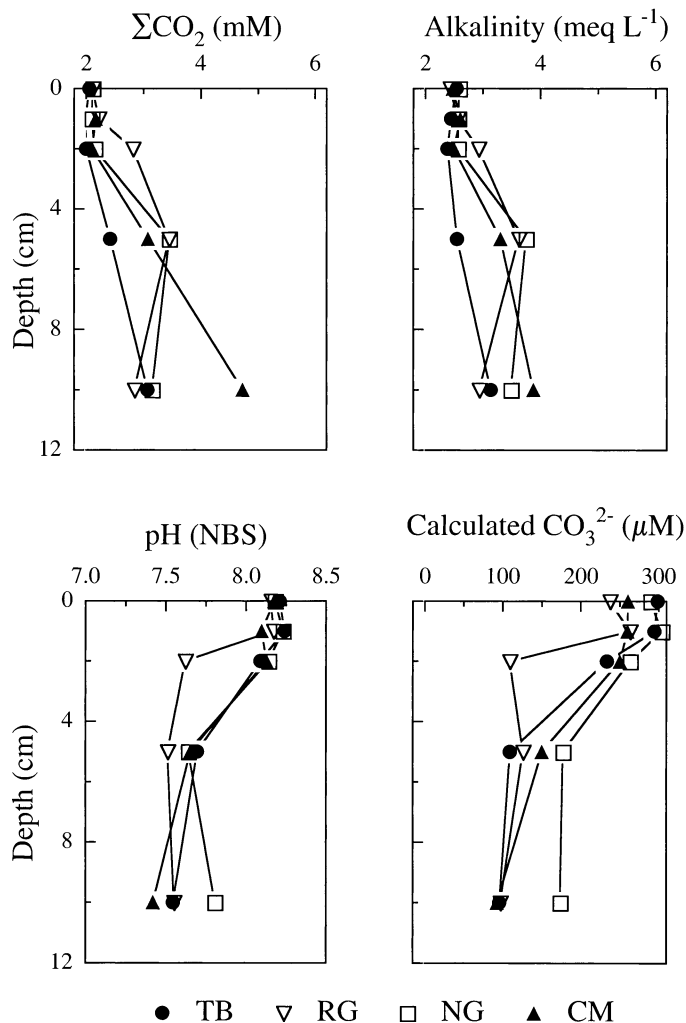


Fig. 3. Pore water profiles of  $\Sigma\text{CO}_2$ , alkalinity, pH, and calculated carbonate ion concentration at the Twin Beaches (TB), Rainbow Gardens (RG), Norman's Grapestones (NG), and Channel Marker (CM) sites. These profiles were collected during LSI 2 (January 1999).

cant transport process down to at least several centimeters deep (Huettel and Webster 2001).

Dissolved oxygen measurements undertaken during LSI 5 indicated that these sediments remained oxic ( $[\text{O}_2]$  greater than  $\sim 20 \mu\text{M}$ ) down to at least 20-cm sediment depth (Fig. 5), although there were significant gradients in pore water oxygen near the sediment surface. Pore water sulfate concentrations also showed no obvious or consistent changes with depth (Fig. 6). This suggests that there was no significant net sulfate reduction in the upper 20 cm of these sediments. A further indication of the lack of significant net sulfate reduction in LSI sediments is obtained from pore water ammonium profiles (data not shown here), based on the assumption that net ammonium accumulation in these sediments results from net sulfate reduction. Given this assumption, ammonium pore water data predicted a maximum change in sulfate of either  $0.06 \pm 0.06 \text{ mM}$  or  $0.20 \pm 0.21 \text{ mM}$  (independent of sediment-sea grass density), depending on whether the detritus undergoing decomposition originated

from sea grass (C:N ratio = 21.75) or phytoplankton (C:N ratio = 6.6). Similar trends in pore water sulfate concentrations have been observed in other Bahamian carbonate sediments (Morse et al. 1985), which suggests that the oxic conditions in LSI sediments are not unique among tropical carbonate sediments.

*Occurrence of sediment carbonate dissolution*—The pore water profiles of pH and carbonate system parameters discussed above (Figs. 3 and 4) were consistent with the occurrence of carbonate dissolution in LSI sediments. However, the asymptotic carbonate ion concentrations ( $\sim 100$  to  $180 \mu\text{M}$ ; see Table 2) exceeded the saturation carbonate ion concentration (SCIC) values for aragonite ( $\sim 60$  to  $65 \mu\text{M}$  at LSI pore water salinities and temperatures, calculated using aragonite solubility data in Millero 1996). At the same time though, these asymptotic pore water concentrations were within the range of SCIC values for high-Mg calcite ( $\sim 40$  to  $500 \mu\text{M}$ ), determined using solubility data summarized in Morse and Mackenzie (1990). This large range in SCIC values for high-Mg calcite is due to two primary reasons. The first is at any given Mg content there is almost an order of magnitude difference in the reported solubility constants for high-Mg calcites (see the discussion in Morse and Mackenzie 1990 for further details). In part this may be due to differences in the experimental approaches used in various studies, although variability in the physical properties of the high-Mg calcites being studied (e.g., surface characteristics, grain size, etc.) also affects their solubility. The second reason is that within a given set of solubility constants in any one study, the solubility of Mg calcite is also a function of the Mg content of the material. Thus in the absence of more detailed information on the mineralogy, composition (e.g., Mg content), and properties of the carbonate minerals undergoing dissolution in LSI sediments (e.g., as in the recent study of Hover et al. 2001) it is difficult to examine this problem in further detail. However, the interpretation of these pore water results, as well as the calcium data discussed below, is that they are consistent with the occurrence of preferential dissolution of high-Mg calcite in LSI sediments (also see similar discussions in Morse et al. 1985).

Evidence for the occurrence of carbonate dissolution in LSI sediments is also seen in Fig. 7, where changes in pore water alkalinity (relative to bottom water values) are plotted against similar changes in  $\Sigma\text{CO}_2$  concentrations for all pore waters below 2-cm sediment depth. The slope of the best fit line through the data from all five sampling dates was  $1.04 \pm 0.03$ . A similar plot of this type, with a similar slope, was observed in other carbonate sediments (Moulin et al. 1985), and the slope of this line was interpreted as being indicative of the coupling of aerobic respiration and carbonate dissolution in these sediments (Eq. 4).

Based on the best fit slope and y-intercept values, the  $\Delta\text{Alk}$  versus  $\Delta\Sigma\text{CO}_2$  plot in Fig. 7 has a positive x-intercept of  $149 \pm 28 \mu\text{M} \Sigma\text{CO}_2$ . In their studies, Moulin et al. (1985) interpreted this x-intercept as the amount of aqueous  $\text{CO}_2$  production from aerobic respiration (Eq. 1) needed to titrate the supersaturated pore waters via Eq. 2 and lower the pore water carbonate ion concentration to the point at which car-

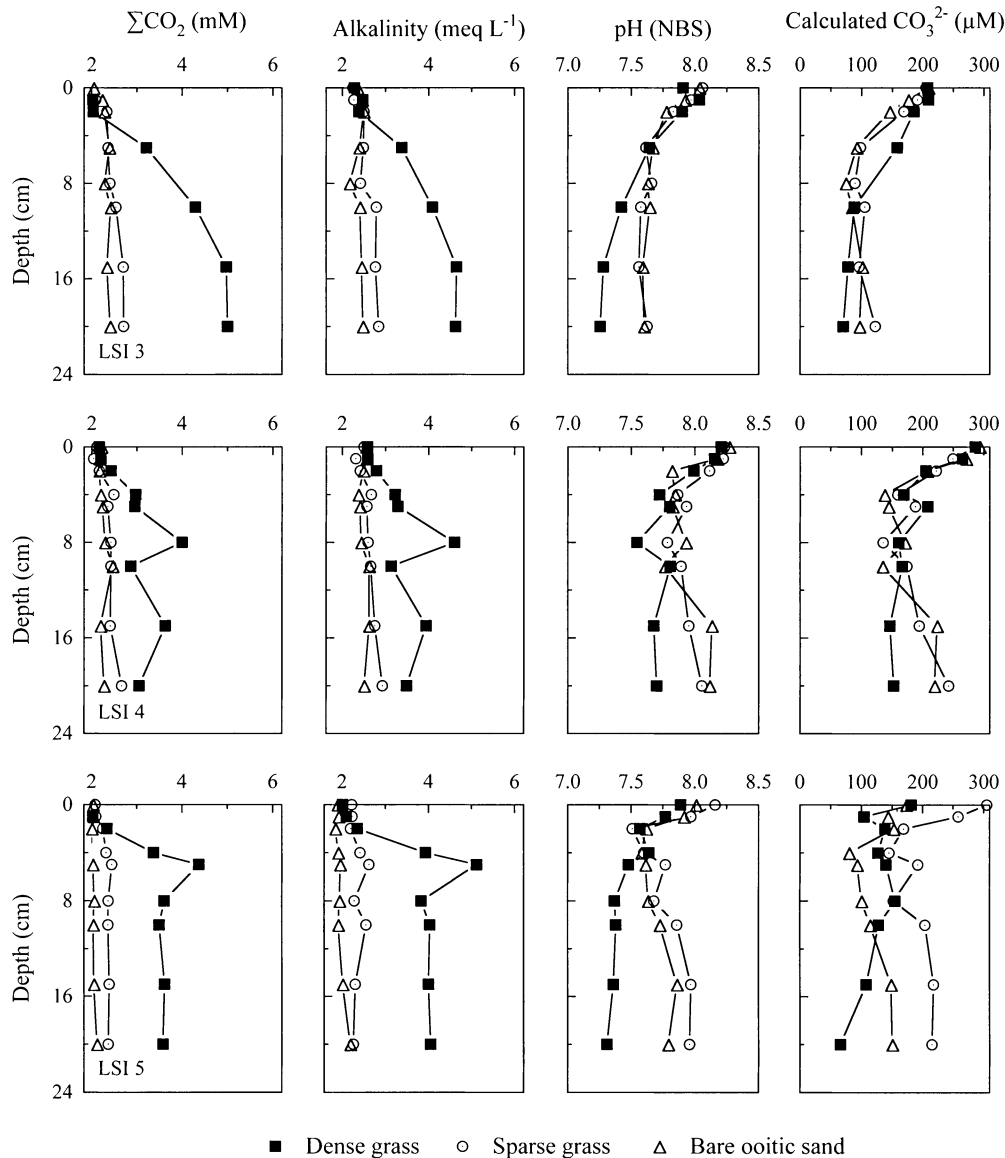


Fig. 4. Average pore water profiles of  $\Sigma\text{CO}_2$ , alkalinity, pH, and calculated carbonate ion concentration from dense turtle grass sediments, sparse turtle grass sediments, and bare oolitic sands, collected during LSI 3 (May 1999, upper panels); LSI 4 (January 2000, middle panels); LSI 5 (May 2000, lower panels). For the LSI 3 profiles the results for dense turtle grass sediments represent average values from four sets of profiles collected at the CM site; for the sparse turtle grass sediments they represent average values from profiles collected at the NG site (two profiles), CM site (one profile), and the RG site (two profiles); for the bare oolitic sands they represent average values from profiles collected at the OS site (two profiles) and the PN site (one profile). For the LSI 4 profiles, the results from dense turtle grass sediments represent average values from profiles collected at the CM site (two profiles) and the RG site (two profiles); for the sparse turtle grass sediments they represent average values from profiles collected at the NG site (one profile), TB site (two profiles), HW site (two profiles), and the BD site (two profiles); for the bare oolitic sands they represent average values from profiles collected at the OS site (one profile) and the PN site (one profile). For the LSI 5 profiles the results from dense turtle grass sediments represent average values from three profiles collected at the CM site; for the sparse turtle grass sediments they represent average values from profiles collected at the CM site (one profile), RG site (two profiles), NG site (two profiles), TB site (one profile), HW site (two profiles), and the WN site (two profiles); for the bare oolitic sands they represent average values from profiles collected at the OS site (two profiles) and the PN site (one profile).

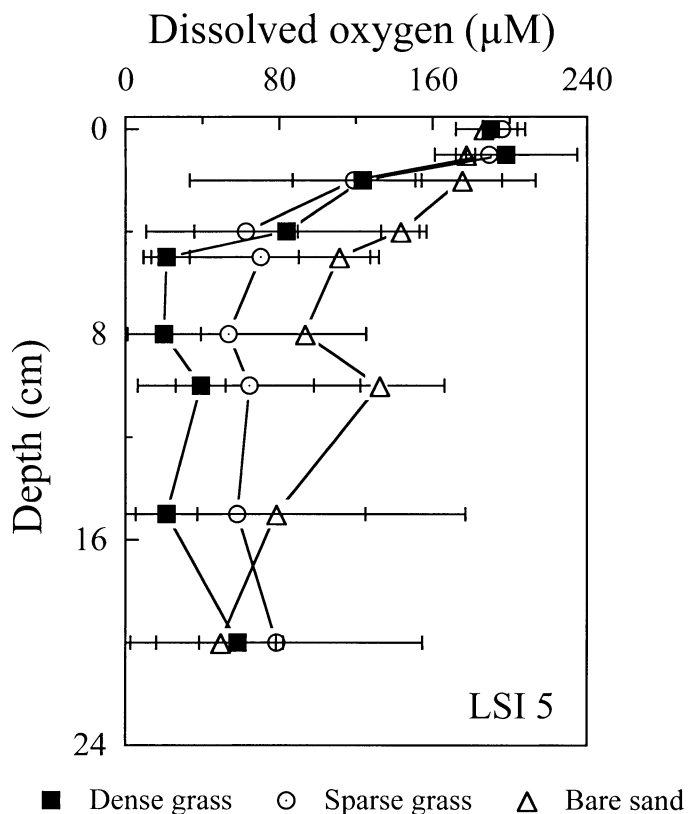


Fig. 5. Average pore water profiles of dissolved oxygen from dense turtle grass sediments, sparse turtle grass sediments, and bare oolitic sands, collected during LSI 5 (May 2000). For the dense grass sediments these results represent average values from three profiles collected at the CM site. For the sparse grass sediments these results represent average values from profiles collected at the NG site (one profile), TB site (one profile), HW site (two profiles), and WN sites (two profiles). For the bare oolitic sands these results represent average values from two profiles collected at the OS site. Error bars are included here to indicate that oxygen concentrations in LSI sediments are greater than zero at depth, in spite of the relatively large standard deviations in these average values.

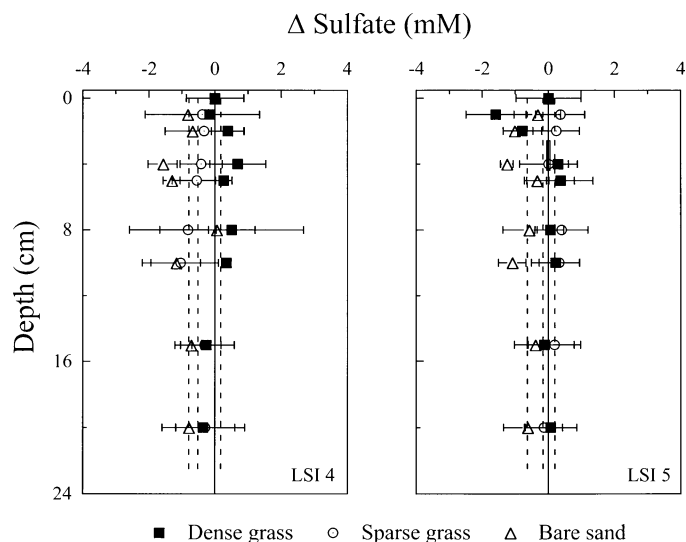


Fig. 6. Depth profiles of  $\Delta$ Sulfate from dense turtle grass sediments, sparse grass sediments, and bare oolitic sands, collected during LSI 4 (left) and LSI 5 (right).  $\Delta$ Sulfate was calculated using the equation  $\Delta\text{sulfate} = [\text{SO}_4^{2-}]_{\text{meas}} - ([\text{salinity}]_{\text{meas}} \cdot ([\text{SO}_4^{2-}]/[\text{salinity}]_{\text{bottom water}}))$  where the measured values are pore water values and the bottom water ratio is an average value based on all bottom water samples collected during that sampling trip. Given the relatively large background sulfate concentrations ( $\sim 30$  mM) as compared to the changes observed here, this approach allowed us to differentiate between small changes in pore water sulfate concentrations due to net in situ bacterial sulfate reduction from those that are due to pore water salinity variations. The profiles used to calculate these average values for each sampling trip are the same as those listed in the caption to Fig. 4. Error bars are included here to indicate that virtually all of these individual  $\Delta$ sulfate values are indistinguishable from zero. The dashed lines shown in each plot are the average  $\Delta$ sulfate values for each sediment type. It can be seen that these averages are all essentially zero and within the uncertainty in the bottom water (BW)  $\Delta$ sulfate values ( $0.0 \pm 0.9$  mM (BW) vs.  $0.2 \pm 0.4$  mM,  $-0.5 \pm 0.3$  mM and  $0.8 \pm 0.5$  mM for LSI 4 dense, sparse, and bare sediments;  $0.0 \pm 1.0$  mM (BW) vs.  $-0.2 \pm 0.7$  mM,  $0.2 \pm 0.2$  mM, and  $-0.6 \pm 0.4$  mM for LSI 5 dense, sparse, and bare sediments).

Table 2. Pore water carbonate data fitting results.

Sampling trip (date)	Bottom water $[\text{CO}_3^{2-}]$ ( $\mu\text{M}$ )*	Asymptotic pore water $[\text{CO}_3^{2-}]$ ( $\mu\text{M}$ )†	Bottom water $[\text{CO}_3^{2-}]$ minus the $x$ -intercept $\Sigma\text{CO}_2$ ( $\mu\text{M}$ )‡
LSI 1 (May 1998)		NC	
LSI 2 (Jan 1999)	$270 \pm 26$	$128 \pm 32$	$121 \pm 45$
LSI 3 (May 1999)	$200 \pm 47$	$92 \pm 21$	$51 \pm 35$
LSI 4 (Jan 2000)	$287 \pm 33$	$177 \pm 61$	$138 \pm 69$
LSI 5 (May 2000)	$228 \pm 99$	$147 \pm 47$	$79 \pm 55$
Average		$136 \pm 36$	$97 \pm 40$

\* Calculated using the program CO2SYS (Lewis and Wallace 1998) as described in the text.

† Based on pore water profiles shown in Figs. 3 and 4.

‡ The  $x$ -intercept  $\Sigma\text{CO}_2$  is obtained from Fig. 7 and equals  $149 \pm 28$   $\mu\text{M}$ .

NC = not calculated due to the lack of pH and salinity data for these pore waters.

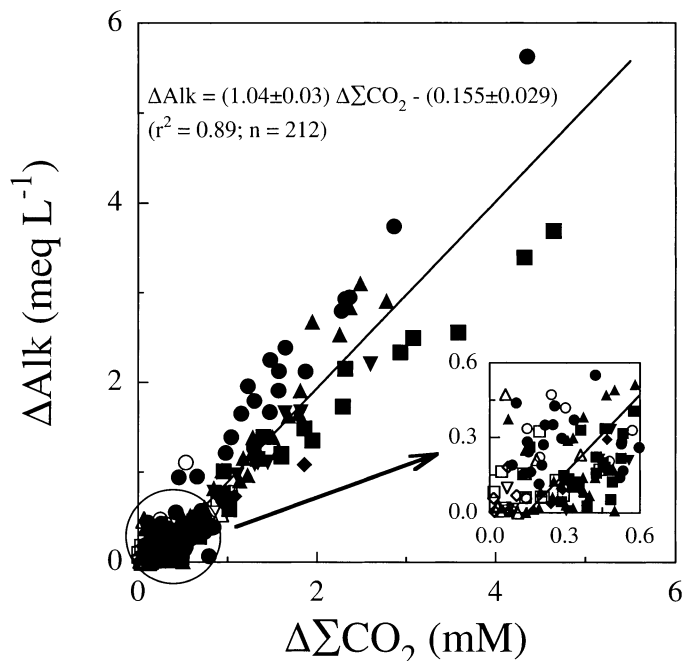


Fig. 7. Changes in pore water alkalinity and  $\Sigma\text{CO}_2$  (both relative to bottom water values) for samples collected in the upper 20 cm of sediments at all sites during the five LSI sampling trips.  $\Delta\text{Alk}$  and  $\Delta\Sigma\text{CO}_2$  were calculated using the same approach used to calculate  $\Delta\text{sulfate}$  (see the caption to Fig. 6 for further details). Filled symbols represent samples collected below 2-cm sediment depth. The best fit line shown here is based on the linear least squares fit of these data, and an analysis of variance (ANOVA) indicated that these slope and  $y$ -intercept values were significant at the  $p < 0.001$  level. Open symbols represent samples collected at 1 and 2 cm sediment depth. They were not included in the regression since they are more likely to represent samples in which changes in alkalinity and  $\Sigma\text{CO}_2$  occur as the pore waters approach saturation with the dissolving carbonate mineral phase (see text for further details). The fact that they do not fall on the  $x$ -axis is in part related to analytical uncertainties and in part to the fact that these values represent small differences between similar numbers.

bonate mineral dissolution occurs. To examine this suggestion, we performed a calculation in which we simply lowered the bottom water carbonate ion concentrations in Table 2 by this  $x$ -intercept amount of aqueous  $\text{CO}_2$  using Eq. 2. The resulting value ( $\sim 100 \mu\text{M}$ ) is similar to the asymptotic pore water carbonate ion concentrations seen in LSI sediments, which roughly represents the carbonate ion concentration in the sediments at which carbonate dissolution occurs. This similarity suggests that the interpretation of the  $x$ -intercept in such plots as proposed by Moulin et al. (1985) is consistent with our understanding of geochemical processes in LSI sediments. The fact that carbonate ion concentrations calculated with bottom water values and this  $x$ -intercept  $\text{CO}_2$  concentration are also slightly lower (in general) than the asymptotic carbonate concentrations in the pore waters implies that the initial  $\text{CO}_2$  added to the pore waters does not react completely with carbonate ion via Eq. 2, which is also consistent with the nature of the buffering reactions in the  $\text{CO}_2$  system.

One potential complicating factor in the interpretation of

this  $\Delta\text{Alk}$  versus  $\Delta\Sigma\text{CO}_2$  plot is the occurrence of anoxic conditions and bacterial sulfate reduction in these sediments (e.g., Hammond et al. 1999). If we express sulfate reduction as



then this process also produces alkalinity and  $\Sigma\text{CO}_2$  in roughly a 1:1 ratio in the absence of any carbonate dissolution. Furthermore, the alkalinity produced by extensive sulfate reduction (greater than  $\sim 4$  to 10 mM sulfate reduced) generally leads to carbonate mineral supersaturation (Morse and Mackenzie 1990). However, as discussed in the previous section, pore water oxygen and sulfate profiles suggest that net sulfate reduction is not significant in these sediments.

In sediments such as those at LSI, any sulfate reduction that does occur in, e.g., reduced sediment microzones must be tightly coupled in situ to sulfide oxidation to prevent the formation of a sulfate pore water gradient (Fig. 6). In their studies of Florida Bay sediments, Ku et al. (1999) observed such a tight in situ coupling between sulfate reduction and sulfide oxidation using rate measurements and pore water concentration and isotope measurements. This then leads to no apparent net sulfate reduction, sulfide mineral formation, or pore water sulfate depletion in these sediments. Under such circumstances, any sulfide produced by bacterial sulfate reduction (Eq. 5) is reoxidized to sulfate by  $\text{O}_2$ , and the net result of the two processes is that sulfate simply acts to shuttle electrons between oxygen and sediment organic matter. More importantly, though, a coupling between sulfate reduction (and its resulting bicarbonate production) and sulfide oxidation (and its resulting proton production) simply results in  $\text{H}_2\text{CO}_3$  (aqueous  $\text{CO}_2$ ) production. Thus from the standpoint of the carbonate system and sediment carbonate dissolution, this is identical to that which occurs from aerobic respiration of sediment organic matter (Eq. 1).

Finally, pore water calcium measurements made during LSI 5 provide additional evidence for the occurrence of sediment carbonate dissolution. Calcium concentrations increased with depth in LSI sediments (Fig. 8), most strongly in dense turtle grass sediments (also see the discussion in the next section), presumably as a result of sediment carbonate dissolution. A plot of changes in calcium versus changes in alkalinity (Fig. 9) had a slope ( $\Delta\text{Ca}^{2+}/\Delta\text{Alk}$ ) of  $0.36 \pm 0.04$ , a value that is similar to, though slightly lower than, the value of 0.5 predicted by Eq. 4. In large part, this difference is likely related to preferential dissolution of high-Mg calcite in these sediments, as discussed above. Skeletal (biogenic) high-Mg calcite can have up to 30 mole percentage Mg (see summary in Morse and Mackenzie 1990) and, for example, the dissolution of 20 mole percentage Mg calcite would decrease the  $\Delta\text{Ca}^{2+}/\Delta\text{Alk}$  ratio from 0.5 to 0.4, consistent with the results in Fig. 9. Adsorption of  $\text{Ca}^{2+}$  to carbonate minerals (Cai et al. 2002) may also help explain why this value of  $\Delta\text{Ca}^{2+}/\Delta\text{Alk}$  is less than 0.5. Again, studies of the mineralogy and surface chemistry of LSI carbonate sediments will be needed to further examine this problem.

*Carbonate dissolution as a function of sea grass density—*The largest pore water alkalinity,  $\Sigma\text{CO}_2$ , and  $\text{Ca}^{2+}$  gradients were observed in sediments underlying dense turtle grass

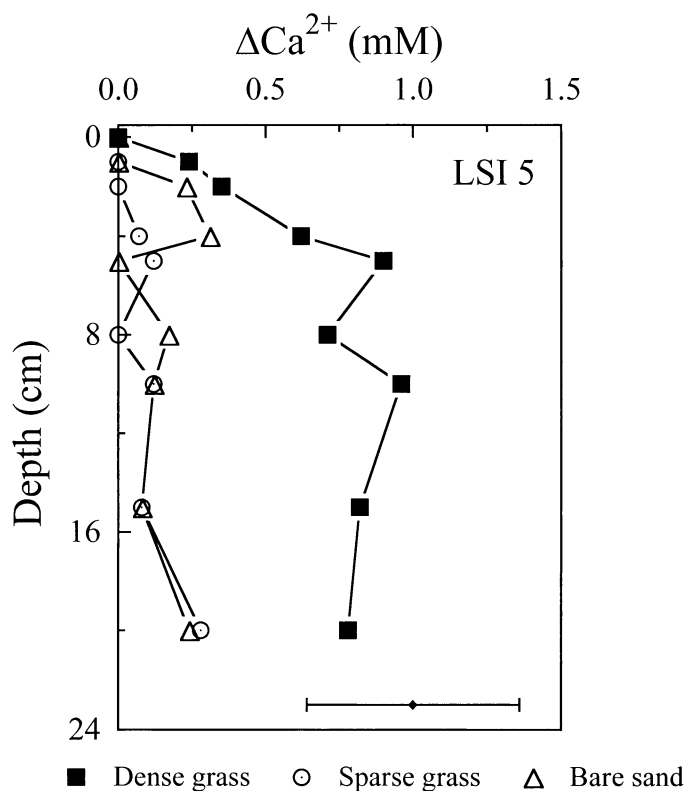


Fig. 8. Average pore water profiles of  $\Delta\text{Ca}^{2+}$  from dense turtle grass sediments, sparse turtle grass sediments, and bare oolitic sands, collected during LSI 5 (May 2000). Shown along the bottom of the figure is the average uncertainty in these  $\Delta\text{Ca}^{2+}$  values. The profiles used to calculate these average values for each sampling trip are the same as those listed in the legend to Fig. 4.  $\Delta\text{Ca}^{2+}$  was calculated using the equation  $\Delta\text{Ca}^{2+} = [\text{Ca}^{2+}]_{\text{meas}} - ([\text{salinity}]_{\text{meas}} \cdot ([\text{Ca}^{2+}]/[\text{Salinity}])_{\text{bottom water}})$ , where the measured values are pore water values and the bottom water ratio is an average value based on all bottom water samples collected during LSI 5. Given the relatively large background  $\text{Ca}^{2+}$  concentrations ( $\sim 11$  mM) as compared to the changes observed here, this approach allowed us to distinguish between small changes in pore water calcium concentrations due to carbonate dissolution from those that are due to pore water salinity variations.

meadows, and the smallest pore water gradients were observed in bare oolitic sands (Figs. 4 and 8). Pore water profiles in sediments underlying sparse turtle grass sediments were closer in magnitude to bare oolitic sands than sediments underlying dense turtle grasses.

In contrast, pH and calculated carbonate ion concentration profiles varied much less as a function of turtle grass density. Therefore, while there was evidence of some carbonate dissolution in all LSI sediments independent of turtle grass density (as inferred from similar trends in pH and carbonate ion profiles), the magnitude of dissolution (as inferred from differences in the alkalinity,  $\Sigma\text{CO}_2$  and  $\text{Ca}^{2+}$  profiles) was strongly related to turtle grass density. Similar differences in pore water chemistry were also seen by Morse et al. (1987) in transects across other Bahamian sea grass beds, based on single pore water samples collected at 40-cm sediment depth.

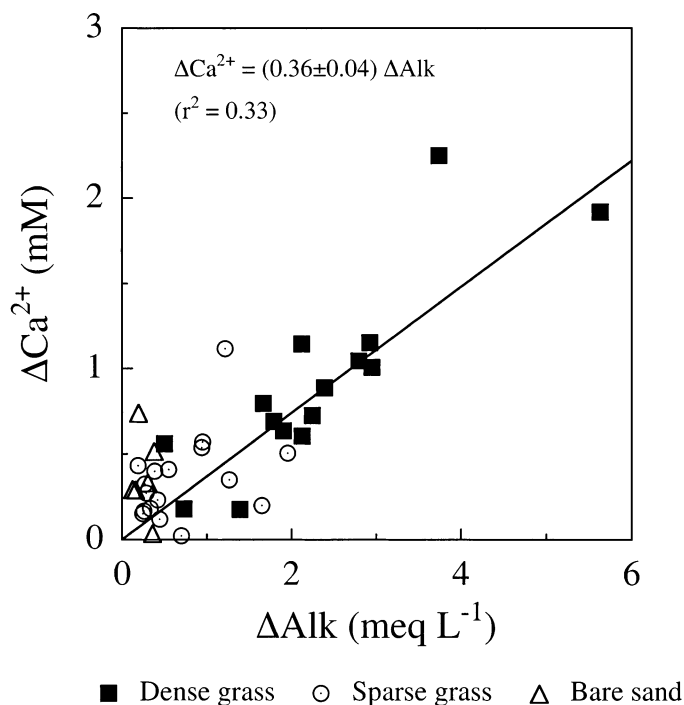


Fig. 9. Changes in pore water calcium and alkalinity (both relative to bottom water values) at all sites for samples collected during LSI 5.  $\Delta\text{Ca}^{2+}$  was calculated as described in the caption to Fig. 8, and  $\Delta\text{Alk}$  was calculated as described in the caption to Fig. 7. Only values from sediment depths greater than 2 cm are shown here (and were included in the regression) for reasons discussed in the legend to Fig. 7. Analysis of variance (ANOVA) indicated that the slope of the best fit line was significant at the  $p < 0.01$  level.

To further examine the effect of turtle grass density on sediment biogeochemical processes, we used these pore water data to estimate diffusive  $\text{O}_2$  fluxes into LSI sediments and depth-integrated rates of SOM oxidation ( $C_{\text{ox}}$ ) and calcium carbonate dissolution (Table 3). Assuming the 1 : 1 stoichiometry between  $\text{O}_2$  consumption and SOM oxidation in Eq. 1 and that sulfate reduction is not an important *net* process in these sediments, diffusion supplied only  $\sim 50\%$  of the  $\text{O}_2$  needed for SOM remineralization in densely vegetated sediments. Since SOM respiration ultimately drives car-

Table 3. A comparison of diffusive  $\text{O}_2$  fluxes, and sediment carbon oxidation rates and sediment carbonate dissolution rates (calculated from pore water diffusive fluxes).

	Dense grasses	Sparse grasses	Oolitic sands (no grasses)
$\text{O}_2$ flux*†	$0.47 \pm 0.17$	$0.23 \pm 0.03$	$0.08 \pm 0.01$
$C_{\text{ox}}*\ddagger$	$0.88 \pm 0.24$	$0.28 \pm 0.10$	$0.06 \pm 0.02$
Carbonate diss'l'n.*‡	$0.94 \pm 0.23$	$0.18 \pm 0.10$	$0.01 \pm 0.01$
$\text{O}_2$ flux/ $C_{\text{ox}}$	$0.54 \pm 0.24$	$0.81 \pm 0.32$	$1.32 \pm 0.48$
Carbonate diss'l'n./ $C_{\text{ox}}$	$1.06 \pm 0.39$	$0.67 \pm 0.43$	$0.24 \pm 0.17$

\* Units of  $\text{mmol m}^{-2} \text{d}^{-1}$ . The  $\text{O}_2$  flux is into the sediments.

† Calculated with  $\text{O}_2$  data from LSI 5 as described in the text.

‡ Calculated with alkalinity and  $\Sigma\text{CO}_2$  diffusive fluxes from LSI 3–5 as described in the text.

bonate dissolution (Eq. 4), this discrepancy is similar to that observed in Florida Bay sediments (Ku et al. 1999). The transport of photosynthetically derived  $O_2$  into the sediments by sea grasses very likely provides the remaining  $O_2$  required to balance carbon oxidation in these sediments.

The discrepancy between  $O_2$  fluxes and  $C_{ox}$  also increased as turtle grass density increased (Table 3). Higher  $C_{ox}$  values in densely vegetated sediments further indicated that turtle grasses either promoted the deposition of water column organic detritus to the sediments and/or served as a source of sediment organic matter themselves (*see* Boschker et al. 2000 and Holmer et al. 2001 for contrasting observations relevant to this issue). In dense and sparse turtle grass sediments, carbon oxidation and carbonate dissolution also appeared to be tightly coupled as predicted by Eq. 4 (i.e., their ratio is  $\sim 1$ ). In bare oolitic sands the low rates of sediment processes and the uncertainty in calculated rates and fluxes make it difficult to know how to interpret the low ratio of carbonate dissolution to carbon oxidation.

At the same time though, the absolute values of the rates and fluxes in Table 3 are almost certainly lower limits of their true values. In part this is because these values are based on pore water gradients in the upper 5 cm of sediment that are themselves likely underestimates of their true value. Similarly, these calculations do not account for any potential pore water advection. Evidence for the occurrence of these advective processes comes in part from the calculated sediment permeabilities discussed above. Additional evidence for this type of advection comes from a comparison of these estimates of sediment carbonate dissolution rates based on diffusive alkalinity fluxes with rates determined directly in whole sediment core incubations. For LSI sediments collected at sparse turtle grass sites, calculated carbonate dissolution rates based on the diffusive alkalinity flux were  $\sim 0.2 \text{ mmol m}^{-2} \text{ d}^{-1}$  (Table 3). In contrast, directly measured rates of sediment carbonate dissolution based on core incubations with sparse turtle grass sediments carried out during LSI 4 and 5 were 15- to 25-fold higher, ranging from 3.5 to 5.3  $\text{mmol m}^{-2} \text{ d}^{-1}$  (Burdige unpubl. data). Such results provide strong evidence for the importance of processes other than molecular diffusion in controlling material fluxes out of these sediments (*see* similar discussions in Marinelli et al. 1998). In light of these observations, determination of the absolute values of the rates and fluxes in Table 3 will require further work. At the same time though, because of the way that advective processes affect concentrations of dissolved constituents in these sediments (*see* the Introduction for further details) we believe that the ratios of these values in Table 3 are less uncertain and provide insight into the role of sea grass-derived  $O_2$  on biogeochemical processes in these sediments.

Finally, Fig. 10 illustrates another way that turtle grass  $O_2$  transport affects sediment carbonate dissolution. Changes in pore water alkalinity and  $O_2$  should fall along the 2:1 line shown here if the concentrations of these quantities are linked by Eq. 4, and the same transport processes (e.g., advection or diffusion) simultaneously transport  $O_2$  into, and alkalinity out of, LSI sediments. However, we see that the data in this figure clearly move away from this 2:1 line in sediments containing higher densities of turtle grasses. Thus,

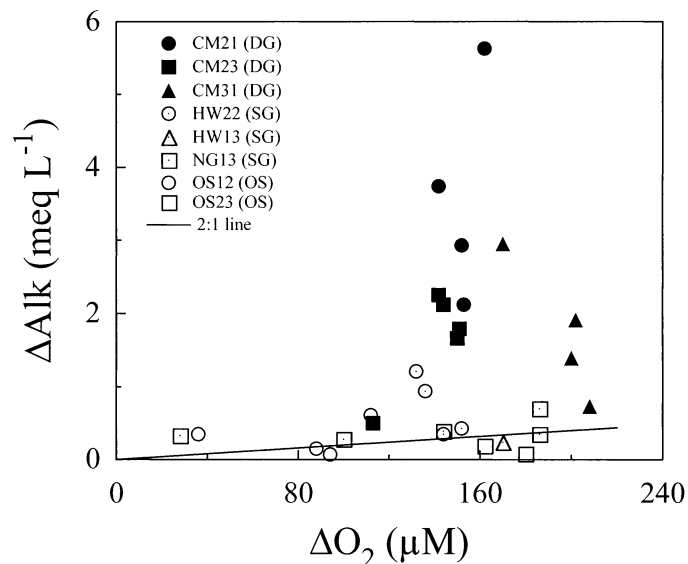


Fig. 10. Changes in pore water  $O_2$  versus alkalinity (both relative to bottom water values) below 5-cm sediment depth at bare oolitic sand (OS, open symbols), sparse turtle grass (SG, dotted symbols), and dense turtle grass (DG filled symbols) sites, collected during LSI 5. Also shown is the 2:1 line for the relationship between these quantities predicted by Eq. 4.

additional  $O_2$  input is required in sparse and dense sea grass sediments to drive the observed sediment carbonate dissolution (i.e., this excess alkalinity production seen in these sediments). More importantly, these results also require that there be an uncoupling between alkalinity removal and  $O_2$  input in these sediments.

We believe that the transport of photosynthetically derived  $O_2$  into the sediments from turtle grass roots and rhizomes is the most likely explanation for these observations. Interestingly, however, the discrepancy between  $\Delta\text{Alk}$  and  $\Delta O_2$  values for dense turtle grass sediments seen in Fig. 10 is substantially greater than the factor of  $\sim 2$  predicted by the results in Table 3. This may occur because the fluxes and ratios reported in Table 3 are controlled not only by molecular diffusion and turtle grass  $O_2$  transport coupled to Eq. 4, but also by pore water advective processes. It therefore appears that advective processes act to partially damp out the impact of sea grass  $O_2$  transport on near-surface pore water profiles and, more importantly, on the resulting rates and fluxes calculated with near-surface pore water gradients.

*The impact of sea grasses on sediment carbonate dissolution*—Based on results presented here, sea grasses appear to facilitate carbonate dissolution in shallow water tropical sediments in at least three ways. First, these highly productive ecosystems (Hemminga and Duarte 2000) can be a major source of SOM for the metabolic (or respiratory) generation of acid (aqueous  $CO_2$ ) that drives carbonate dissolution. Second, the overlying leaf canopy dampens water motion and promotes the flux of inorganic and organic particles to the sediments, particularly in areas dominated by strong tidal currents (Fonseca and Fisher 1986; Koch and Gust 1999; Gacia et al. 1999). Finally, the input of photo-

synthetically produced  $O_2$  from roots and rhizomes may drive the production of the respiratory acid that dissolves carbonate minerals. However, unlike aquatic plants with emergent stems and leaves, fully submersed sea grasses release  $O_2$  to the rhizosphere only when there is sufficient light for photosynthesis (Smith et al. 1984; Pedersen et al. 1998). Consequently, the flux of  $O_2$  into the sediments will depend on shoot density, the total area of photosynthetic leaves, and the incident photon flux to drive photosynthesis. Furthermore, this  $O_2$  flux will exhibit a strong diurnal cycle that may also have important implications on the daily integrated rates of sediment carbon oxidation and carbonate dissolution.

Oxygen input from sea grass roots can have a significant impact on redox conditions in the rhizosphere of anoxic clastic sediments and promote the oxidation of potential toxic reduced metabolites such as sulfide,  $Fe^{2+}$ , and  $Mn^{2+}$  (Jaynes and Carpenter 1986; Kemp and Murray 1986; Lee and Dunton 2000). In contrast, there have been far fewer studies examining the effects of  $O_2$  input from sea grasses on the biogeochemistry of tropical carbonate sediments. In addition to the effects described here (and also discussed in Ku et al. 1999) sea grass-mediated carbonate dissolution may also play a role in providing the phosphorus required by sea grasses (Jensen et al. 1998). This may occur because a significant fraction of the phosphorus in sea grass sediments is either adsorbed to carbonate minerals or incorporated in mineral phases such as calcium fluoroapatite and can only be made available to the plants by acid-mediated mineral dissolution.

The turtle grass population at LSI was characterized by light-saturated rates of net oxygen production that ranged from  $\sim 60$  and  $110 \mu\text{mol} (\text{g leaf dry weight})^{-1} \text{h}^{-1}$  (Table 1). Assuming that photosynthesis occurred at light-saturated rates for 10 h each day in these shallow clear waters, area-specific rates of net  $O_2$  production should range from  $\sim 60$  (sparse grasses) to  $400$  (dense grasses)  $\text{mmol } O_2 \text{ m}^{-2} \text{ d}^{-1}$ . Based on our preliminary LSI data (*see above*) and published results from Florida Bay (Walter and Burton 1990; Rude and Aller 1991), measured rates of carbonate dissolution in these shallow water carbonate sediments range from  $4$  to  $11 \text{ mmol m}^{-2} \text{ d}^{-1}$ . Given the stoichiometry of Eq. 4, this then implies that less than 15% of the net photosynthetic  $O_2$  produced by these sea grass leaves needs to be released into the sediments to promote carbonate dissolution. This percentage appears reasonable based on observations in the literature for other sea grasses (Sand-Jensen et al. 1982; Smith et al. 1984; Kemp and Murray 1986).

In summary, our results indicate that the input of  $O_2$  from sea grass roots can explain past discrepancies in sediment carbonate dissolution budgets and may provide a mechanism by which these plants mediate carbonate dissolution in shallow water tropical sediments. However, more work is clearly needed to further quantify this linkage between sea grass  $O_2$  transport and sediment carbonate dissolution, as well as its ecological and biogeochemical significance.

Finally, we note that sea grass photosynthesis in seawater is inherently  $CO_2$  limited (Beer 1989; Durako 1993; Zimmerman et al. 1997; Invers et al. 2001). Thus, sea grass productivity may increase in response to rising  $CO_2$  levels

in the atmosphere and surface ocean, increasing both the flux of organic carbon and  $O_2$  into carbonate sediments. Furthermore, remineralization of this sea grass organic matter in sediments, coupled with sediment carbonate dissolution and rapid flushing of the sediment pore waters by physical advection, creates a mechanism for the transfer of atmospheric  $CO_2$  to the oceanic bicarbonate pool, where it should have a residence time on the order of tens of thousands of years (i.e., the residence time of bicarbonate in the oceans). Thus one might expect a positive feedback between rising atmospheric  $CO_2$  and rates of carbonate dissolution in shallow water environments such as the Bahama Banks, which are heavily populated with sea grasses. Overall however, these coupled processes will eventually exert a small negative feedback on rising atmospheric  $CO_2$  levels. At the same time, though, they could have significant impacts on regional and global carbonate sediment budgets.

## References

- ALLER, R. C. 1982. Carbonate dissolution in shallow water marine sediments: Role of physical and biological reworking. *J. Geol.* **90**: 79–95.
- BEER, S. 1989. Photosynthesis and respiration of marine angiosperms. *Aquat. Bot.* **34**: 153–166.
- BERELSON, W. M., J. MCMANUS, T. KILGORE, K. COALE, K. S. JOHNSON, D. BURDIGE, AND C. PILSKALN. 1996. Biogenic matter diagenesis on the sea floor: A comparison between two continental margin transects. *J. Mar. Res.* **54**: 731–762.
- BERG, P., AND K. J. MCGLATHERY. 2001. A high-resolution pore water sampler for sandy sediments. *Limnol. Oceanogr.* **46**: 203–210.
- BERNER, R. A. 1966. Chemical diagenesis of some modern carbonate sediments. *Am. J. Sci.* **264**: 1–36.
- BOSCHKER, H. T. S., A. WIELEMAKER, B. E. M. SCHAUB, AND M. HOLMER. 2000. Limited coupling of macrophyte production and bacterial carbon cycling in the sediments of *Zostera* spp. meadows. *Mar. Ecol. Prog. Ser.* **203**: 181–189.
- BOUDREAU, B. P. 1997. Diagenetic models and their implementation. Springer.
- BURDIGE, D. J., AND J. HOMSTEAD. 1994. Fluxes of dissolved organic carbon from Chesapeake Bay sediments. *Geochim. Cosmochim. Acta* **58**: 3407–3424.
- CAI, W.-J., Y. WANG, AND R. JAHNKE. 2002. Evidence of surface reactions of  $Ca^{2+}$  and inorganic carbon species in seawater. *EOS* **83**: OS11D–62 (abstr.).
- DILL, R. F. 1991. Subtidal stromatolites, ooids and crusted-lime mud beds at the Great Bahama Bank Margin, pp. 147–171. *In* From shoreline to abyss. SEPM Spec. Pub. No. 46.
- DOE. 1994. Handbook of methods for the analysis of the various parameters of the carbon dioxide system in sea water, version 2. *In* A. G. Dickson and C. Goyet [eds.], ORNL/CDIAC-74.
- DURAKO, M. J. 1993. Photosynthetic utilization of  $CO_{2(aq)}$  and  $HCO_3^-$  in *Thalassia testudinum* (Hydrocharitaceae). *Mar. Biol.* **115**: 373–380.
- ELDRIDGE, P. M., AND J. W. MORSE. 2000. A diagenetic model for sediment-seagrass interactions. *Mar. Chem.* **70**: 89–103.
- EMERSON, S., AND M. L. BENDER. 1981. Carbon fluxes at the sediment-water interface: Calcium carbonate preservation. *J. Mar. Res.* **39**: 139–162.
- FONSECA, M. S., AND J. S. FISHER. 1986. A comparison of canopy friction and sediment movement between four species of seagrass with reference to their ecology and restoration. *Mar. Ecol. Prog. Ser.* **29**: 15–22.

- GACIA, E., T. GRANATA, AND C. M. DUARTE. 1999. An approach to measurement of particle flux and sediment retention within seagrass (*Posidonia oceanica*) meadows. *Aquat. Bot.* **65**: 255–268.
- GIESKES, J. M., T. GAMO, AND H. BRUMSACK. 1991. Chemical methods for interstitial water analysis aboard JOIDES RESOLUTION. Ocean Drilling Program. Tech. Note 15.
- HAMMOND, D. E., P. GIODANI, W. M. BERELSON, AND R. POLETTI. 1999. Diagenesis of carbon and nutrients and benthic exchange in sediments of the northern Adriatic Sea. *Mar. Chem.* **66**: 53–97.
- HEMMINGA, M. A., AND C. M. DUARTE. 2000. Seagrass ecology. Cambridge Univ. Press.
- HOLMER, M., F. Ø. ANDERSEN, S. L. NIELSEN, AND H. T. S. BOSCHKER. 2001. The importance of mineralization based on sulfate reduction for nutrient regeneration in tropical seagrass sediments. *Aquat. Bot.* **71**: 1–17.
- HOVER, V. C., L. M. WALTER, AND D. R. PEACOR. 2001. Early marine diagenesis of biogenic aragonite and Mg-calcite: New constraints from high-resolution STEM and AEM analyses of modern platform carbonates. *Chem. Geol.* **175**: 221–248.
- HUETTEL, M., AND I. T. WEBSTER. 2001. Porewater flow in permeable sediments, p. 144–179. *In* B. P. Boudreau and B. B. Jørgensen [eds.], *The benthic boundary layer*. Oxford Univ. Press.
- INVERS, O., R. ZIMMERMAN, R. ALBERTE, M. PEREZ, AND J. ROMERO. 2001. Inorganic carbon sources for seagrass photosynthesis: An experimental evaluation for bicarbonate use in temperate species. *J. Exp. Mar. Biol. Ecol.* **265**: 203–217.
- JAYNES, M. L., AND S. R. CARPENTER. 1986. Effects of vascular and nonvascular macrophytes on sediment redox and solute dynamics. *Ecology* **67**: 875–882.
- JENSEN, H. S., K. J. MCGLATHERY, R. MARINO, AND R. W. HOWARTH. 1998. Forms and availability of sediment phosphorus in carbonate sands of Bermuda seagrass beds. *Limnol. Oceanogr.* **43**: 799–810.
- KEMP, W. M., AND L. MURRAY. 1986. Oxygen release from roots of the submersed macrophyte *Potamogeton Perfoliatus* L.: Regulating factors and ecological implications. *Aquat. Bot.* **26**: 271–283.
- KOCH, E., AND G. GUST. 1999. Water flow in tide- and wave-dominated beds of the seagrass *Thalassia testudinum*. *Mar. Ecol. Prog. Ser.* **184**: 63–72.
- KU, T. C. W., L. M. WALTER, M. L. COLEMAN, R. E. BLAKE, AND A. M. MARTINI. 1999. Coupling between sulfur recycling and syndepositional carbonate dissolution: Evidence from oxygen and sulfur isotope compositions of pore water sulfate, South Florida platform, USA. *Geochim. Cosmochim. Acta* **63**: 2529–2546.
- LEE, K.-S., AND K. H. DUNTON. 2000. Diurnal changes in pore water sulfide concentrations in the seagrass *Thalassia testudinum* beds: The effects of seagrasses on sulfide dynamics. *J. Exp. Mar. Biol.* **255**: 201–214.
- LEWIS, E., AND D. W. R. WALLACE. 1998. Program developed for CO<sub>2</sub> system calculations. Oak Ridge National Laboratory. ORNL/CDIAC-105.
- LUSTWERK, R. L., AND D. J. BURDIGE. 1995. Elimination of dissolved sulfide interference in the flow injection determination of ΣCO<sub>2</sub> by the addition of molybdate. *Limnol. Oceanogr.* **40**: 1011–1012.
- MARINELLI, R. L., R. A. JAHNKE, D. B. CRAVEN, J. R. NELSON, AND J. E. ECKMAN. 1998. Sediment nutrient dynamics on the South Atlantic Bight continental shelf. *Limnol. Oceanogr.* **43**: 1305–1320.
- MILLERO, F. J. 1996. Chemical oceanography, 2nd ed. CRC.
- MILLIMAN, J. D. 1993. Production and accumulation of calcium carbonate in the ocean: Budget of a nonsteady state. *Glob. Biogeochem. Cycles* **7**: 927–957.
- MORSE, J. W., AND F. W. MACKENZIE. 1990. Geochemistry of sedimentary carbonates. Elsevier.
- , J. J. ZULLIG, L. D. BERNSTEIN, F. J. MILLERO, P. MILNE, A. MUCCI, AND G. R. CHOPPIN. 1985. Chemistry of calcium carbonate-rich shallow water sediments in the Bahamas. *Am. J. Sci.* **285**: 147–185.
- , ———, R. L. IVERSON, G. R. CHOPPIN, A. MUCCI, AND F. J. MILLERO. 1987. The influence of seagrass beds on carbonate sediments in the Bahamas. *Mar. Chem.* **22**: 71–83.
- MOULIN E., A. JORDENS, AND R. WOLLAST. 1985. Influence of the aerobic bacterial respiration on the early dissolution of carbonates in coastal sediments. *Progr. Belgium Ocean. Res.*, Brussels pp. 196–205.
- PEDERSEN, O., J. BORUM, C. M. DUARTE, AND M. D. FORTES. 1998. Oxygen dynamics in the rhizosphere of *Cymodocea rotundata*. *Mar. Ecol. Prog. Ser.* **169**: 283–288.
- ROY, R. N., L. N. ROY, K. M. VOGEL, C. PORTER-MOORE, T. PEARSON, C. E. GOOD, F. J. MILLERO, AND D. M. CAMPBELL. 1996. Erratum to The dissociation constants of carbonic acid in seawater at salinities 5 to 45 and temperatures 0 to 45°C. *Mar. Chem.* **52**: 183.
- RUDE, P. D., AND R. C. ALLER. 1991. Fluorine mobility during early diagenesis of carbonate sediments: An indicator of mineral transformations. *Geochim. Cosmochim. Acta* **55**: 2491–2509.
- SAND-JENSEN, K., C. PRAHL, AND H. STOKHOLM. 1982. Oxygen release from roots of submerged aquatic macrophytes. *Oikos* **38**: 349–454.
- SMITH, R. D., W. C. DENNISON, AND R. S. ALBERTE. 1984. Role of seagrass photosynthesis in root aerobic processes. *Plant Physiol.* **74**: 1055–1058.
- ULLMAN, W. J., AND R. C. ALLER. 1982. Diffusion coefficients in nearshore marine sediments. *Limnol. Oceanogr.* **27**: 552–556.
- WALTER, L. M., S. A. BISHOP, W. P. PATTERSON, AND T. W. LYONS. 1993. Dissolution and recrystallization in modern carbonates: Evidence from pore water and solid phase chemistry. *Philos. Trans. R. Soc. Lond.*, A **344**: 27–36.
- , AND E. A. BURTON. 1990. Dissolution of recent platform carbonate sediments in marine pore fluids. *Am. J. Sci.* **290**: 601–643.
- WEBB, W., M. NEWTON, AND D. STARR. 1974. Carbon dioxide exchange of *Alnus rubra*: A mathematical model. *Oecologia* **17**: 281–291.
- ZIMMERMAN, R. C., J. B. SOOHOO, J. N. KREMER, AND D. Z. D. D'ARGENIO. 1987. Evaluation of variance approximation techniques for non-linear photosynthesis-irradiance models. *Mar. Biol.* **95**: 209–215.

Received: 16 November 2001  
 Accepted: 6 May 2002  
 Amended: 3 June 2002